2025 50th International Conference on Infrared, Millimeter, and Terahertz Waves (IRMMW-THz) | 979-8-3503-7883-2/25/$31.00 ©2025 IEEE | DOI: 10.1109/IRMMW-THz61557.2025.11319597

Towards a Multi-Pixel Terahertz Camera with Passive Sensitivity Integrated in 130nm SiGe BiCMOS

M. Hoogelander, M. Spirito, N. Llombart, M. Alonso-delPino
Delft University of Technology, Delft, The Netherlands

***Abstract*—This contribution presents a silicon-integrated focal plane array (FPA) THz camera that achieves passive-level sensitivity and a densely sampled field-of-view. The FPA chip is designed in a 130nm SiGe BiCMOS technology from IHP and consists of a previously presented chessboard array topology with integrated direct detectors. The detectors are realized using a differential pair of heterojunction bipolar transistors in a common-base configuration biased in deep saturation. A silicon, hyper-hemispherical lens is mounted on the chip as a primary focusing element. The maximum responsivity of the camera is simulated to be 680 V/W at 350GHz, and above half this value between 260GHz and 600GHz. Simulations show that the minimum NEP is on the order of 2pW/$\sqrt{Hz}$, yielding an NETD of 1K for a 150ms integration time. For characterization and future imaging demonstrations, the camera is mounted in a quasi-optical setup, which refocuses the beams from the silicon lens onto an imaging plane. Measurements performed in this setup demonstrate that the camera achieves a responsivity on the order of 550/W, while also realizing a dense focal plane sampling.**

I. Introduction

Recent progress in silicon-integrated, sub-terahertz direct detectors has shown that passive-level temperature resolution on the order of 1K for 1s of integration time can be reached using commercial silicon processes. The state-of-the-art noise-equivalent power (NEP) of CMOS-based designs is now below 10 pW/$\sqrt{\text{Hz}}$ [1], whereas designs in SiGe BiCMOS are even capable of achieving NEP-levels on the order of 2pW/$\sqrt{\text{Hz}}$ [2]. Already, a passive imaging demonstration using an uncooled single-pixel imager integrated in 130nm SiGe BiCMOS has been presented [3]. In order to realize a THz camera useful for commercial imaging applications, however, it is necessary to integrate these detectors in large, densely-sampled focal plane arrays (FPA). Arrays with a large number of pixels [4] and arrays with a near diffraction-limited focal plane sampling [5] have been demonstrated. However, no uncooled, integrated FPAs have been reported yet that achieve passive-level performance.

In this contribution, we present an FPA camera, operating from 250GHz to 600GHz, that excels both in terms of NEP and spatial resolution. To achieve this, we have integrated the densely-sampled chessboard FPA topology from [5] in a high-performance SiGe BiCMOS technology to improve the NEP. For characterization, the THz camera is embedded in a quasi-optical measurement setup from [6].

II. Integrated THz Camera

An overview of the THz camera, consisting of the imaging chip and a silicon lens, and the overall measurement setup is shown in Fig. 1. From left to right, it contains the THz camera, a hyperbolic lens made of HDPE plastic that refocuses the beams from the camera, and a horn antenna placed in the imaging plane to measure the camera response and radiation patterns in the spot.

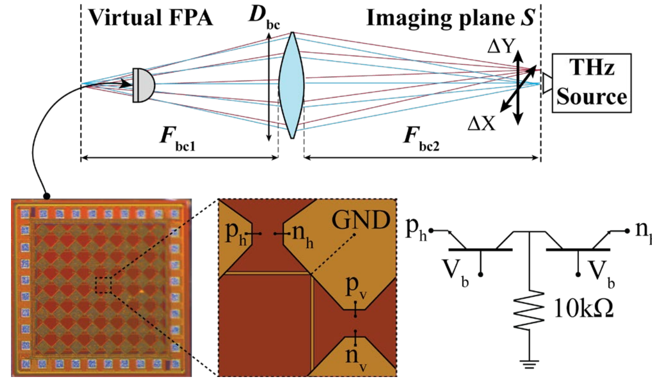

Fig. 1. Overview of the THz camera and measurement setup. The insets depict a picture of the imaging chip and a schematic of the direct detectors

The imaging chip features a chessboard FPA [5] with direct-detectors, integrated in the SiGe SG13G2 process from IHP. An overview of the chip is shown in Fig. 1. Besides the different silicon platform, the main change with respect to [5], in which the chessboard topology was introduced, is in the circuit design of the direct detectors. In this work, the direct detectors are comprised of a differential pair of heterojunction bipolar transistors (HBT) in a deeply saturated common-base configuration, similar to the detector design from [2]. Although possible, it can be challenging to outperform a forward-active biased CB stage in terms of NEP [2]. Biasing in deep saturation, however, has other advantages. First, it consumes less current compared to a forward-active common-base stage and secondly, because only a single bias voltage is required, laying out the on-chip biasing network is much simpler. Both these aspects make it attractive if one want to realize densely sampled, large-scale imaging arrays.

III. Prototype and Characterization

The imaging chip was glued on the base of a silicon, hyper-hemispherical lens, identical to the one in [6]. As explained in [6], the silicon lens transforms the beams from the different FPA elements such that they appear to originate from a virtual focal plane located behind the lens. When this virtual focal plane is aligned with the primary focal plane of the plastic lens, the beams of all FPA elements in the chessboard array are focused to a unique point in the imaging plane, hereby maintaining the scanning functionality of the camera. To be able to couple to both polarizations within the FPA, the camera was rotated such that both polarizations have are at an 45^o angle with respect to the horn.

To simulate the different performance metrics, various CAD tools were used. Keysight ADS was used to simulate responsivity of the standalone detector, as well as its noise contributions. The radiation patterns inside the silicon and the

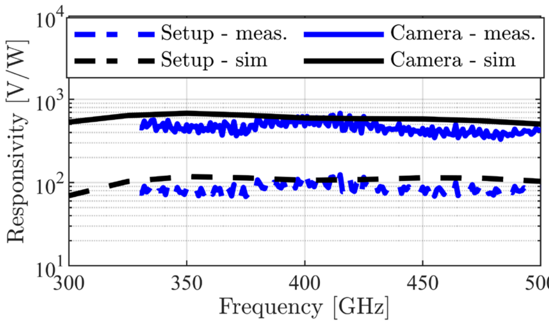

Fig. 2. Measured and simulated responsivity of the camera. The solid lines represent the responsivity of the overall setup, whereas the dashed lines indicate the responsivity if the losses of the QO system are removed.

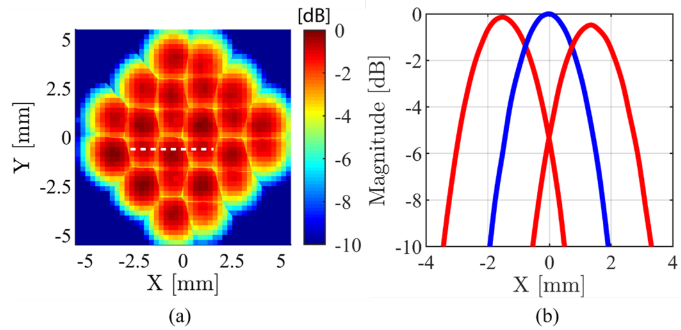

Fig. 3. Measured patterns in the imaging plane at 400GHz. (a) 2D patterns of all 24 pixels in the chessboard FPA. (b) patterns of 3 adjacent pixels along the white cut shown in the 2D pattern

losses of the chessboard FPA were obtained using CST. Subsequently, the results from CST were used as input to an in-house PO tool [7] to find the losses and the patterns radiated by the hyper-hemispherical lens. Combined with the losses of the FPA, these constitute the total losses of the THz camera, η_{Cam}. Finally, TiCRA GRASP was used to propagate these patterns to the imaging plane and find the efficiency of the quasi-optical measurement setup, η_{QO}, which includes the spillover, reflection and ohmic losses from the plastic lens, but also the coupling to the horn. The responsivity of the overall measurement system, $\Re_{v,sys}$, is then found by:

$$\Re_{v,sys} = \eta_{match}\eta_{Cam}\eta_{QO}\Re_{v,det}, \quad (1)$$

where $\Re_{v,det}$ is the voltage responsivity of the standalone detector and η_{match} the efficiency of the impedance matching between the detector and the FPA element.

The simulated responsivity is shown in Fig. 2. The responsivity of the overall setup is on the order of 100V/W, whereas the responsivity of the THz camera (i.e., without η_{QO}) is 680V/W at 350 GHz. The camera operates from 260GHz up to 600GHz, the range in which camera responsivity is higher than half its peak value. Combined with ADS simulations of the detector noise, the NEP of the standalone THz camera is expected to be on the order of 2pW/$\sqrt{Hz}$, with a NETD of 1K for a 150ms integration time.

A. Measurement Results

The radiation patterns and the system responsivity were measured in the imaging plane in the WR2.2 band. To provide power to the horn antenna, a frequency extender module from Virginia Diodes was used. This extender was in turn driven using 100kHz, *on-off* modulated mm-wave signal to prevent SNR deterioration due to low-frequency noise. The (modulated) response of the THz camera was acquired in the frequency domain, using a 40-dB gain low-noise instrumentation amplifier (LNIA) and a set of 14-bit, 100MS/s ADC cards, as explained in [5]. For all measurements, an integration time of 20ms was used per acquisition.

The measured radiation patterns in the spot, at 400GHz, are shown in Fig. 3(a). These radiation patterns where measured by scanning the horn antenna in the imaging plane using a CNC machine. In Fig. 3(b), the radiation patterns of three adjacent pixels are shown along the cut indicated in Fig. 3(a), where the vicinity of the beams demonstrates the excellent spatial resolution of the camera.

The responsivity of the total quasi-optical system, $\Re_{v,sys}$, can be extracted from the voltage response by dividing it by the gain of the LNIA, G_{LNIA}, and the total power radiated by the horn antenna [5]. Fig. 2 shows the measured $\Re_{v,sys}$, for a base-emitter bias voltage of 0.75V. As can be seen, the responsivity is slightly lower than expected, but still within 1dB of simulations. Since the system responsivity highly depends on the radiation pattern and polarization of the horn, evaluating the responsivity at the aperture of the silicon lens would provide a better perspective on the camera performance. To realize this, the simulated η_{QO} is removed in post-processing, of which the result is also shown in Fig. 2. More detailed measurements, for example on the noise performance and NEP, will be presented at the conference.

Acknowledgements

We would like to express our gratitude to the Leibniz Institute for High Performance Microelectronics (IHP) for the technology access and support.

References

[1] F. Ludwig, et al, "Modeling of Antenna-Coupled Si MOSFETs in the Terahertz Frequency Range," in IEEE Transactions on Terahertz Science and Technology, vol. 14, no. 3, pp. 414-423, May 2024.

[2] M. Andree, et al., "Broadband Modeling, Analysis, and Characterization of SiGe HBT Terahertz Direct Detectors," in IEEE Transactions on Microwave Theory and Techniques, vol. 70, no. 2, pp. 1314-1333, Feb. 2022.

[3] M. Andree, J. Grzyb, H. Rücker and U. R. Pfeiffer, "Towards Passive Imaging With Uncooled, Low-NEP SiGe HBT Terahertz Direct Detectors," in *IEEE Transactions on Terahertz Science and Technology*, vol. 14, no. 5, pp. 632-651, Sept. 2024.

[4] R. Al Hadi *et al.*, "A 1 k-Pixel Video Camera for 0.7–1.1 Terahertz Imaging Applications in 65-nm CMOS," in *IEEE Journal of Solid-State Circuits*, vol. 47, no. 12, pp. 2999-3012, Dec. 2012.

[5] M. Hoogelander *et al.*, "Chessboard Focal Plane Array for a CMOS-Integrated Terahertz Camera," in *IEEE Transactions on Terahertz Science and Technology*, vol. 13, no. 6, pp. 704-717, Nov. 2023.

[6] M. Hoogelander, et al., "Demonstration of Near Diffraction-Limited Terahertz Images Using a CMOS-Integrated Chessboard Array," in *IEEE Transactions on Terahertz Science and Technology*, vol. 14, no. 4, pp. 531-536, July 2024.

[7] H. Zhang, et al., "A Fourier Optics Tool to Derive the Plane Wave Spectrum of QuasiOptical Systems [EM Programmer's Notebook]," in IEEE Antennas and Propagation Magazine, vol. 63, no. 1, pp. 103-116, Feb. 2021.